JOINT INSTITUTE FOR NUCLEAR RESEARCH
Department of Raman Spectroscopy, Frank Laboratory of Neutron Physics

FINAL REPORT ON THE SUMMER STUDENT PROGRAM

Raman spectroscopy of powdered magnetite

Supervisor:
Dr. Grigory Arzumanyan

Student:
Angelina Antonova

Participation period:
June 27 – July 16, 2016
August 22 – September 11, 2016

Dubna, 2016

CONTENT

1. Introduction: What is Raman spectroscopy?

Raman spectroscopy and microscopy occupy its own niche in the study of properties, structure and diagnostics of condensed matter. Raman spectroscopy refers to scattered light from a sample that exhibits a frequency shift reflecting the energy of specific molecular vibrations within the sample of interest. In this manner, it provides a detailed chemical composition of the sample – a chemical fingerprint in essence. Raman scattering, as a label-free and noninvasive spectroscopy, is well suited for cell imaging and avoids many of the problems associated with the fluorescence including photo-bleaching and photo-induced damage of living organisms due to the presence of exogenous tags. Using excitation wavelength in the NIR range (typically 785–1064 nm) is capable of measuring Raman spectra from biosamples with minimum interference from fluorescence. Also, Raman spectroscopy is successfully used for geological studies, since it has high spatial resolution and non-destructive properties.

1.1 Historical background

Professors Mandelshtam L.I. and Landsberg G.S. in Moscow launched experiments on the scattering of light in condensed media in 1926. One of the objects of study was crystalline quartz. Intense line of a mercury lamp was applied as a source of exciting radiation. The experiments revealed that weak radiation which frequency is shifted relative to the primary frequency of the exciting radiation is present in the spectrum of the scattered light. Thus, the spectrum has several symmetric 'satellite' frequencies $\omega_0 - \Omega_j$ (Stokes satellite) and $\omega_0 + \Omega_j$ (anti-Stokes satellite) with respect to the exciting radiation frequency ω_0. It was also found that the observed shifts Ω_j of the frequency of the exciting radiation are higher by orders of magnitude than typical values of frequencies of acoustic waves, which was seen as the cause of light scattering in Mandelstam theory. Later it was determined that many other types of waves may be with the wave exciting radiation in addition to the acoustic waves, in particular waves of optical oscillations characterized oncoming traffic type inequivalent atoms crystal primitive cells. That was the cause of the frequency shift of the exciting radiation that was observed in the experiments of Landsberg and Mandelstam. In the future, this type of scattering was called Combinational scattering light.

At the same time (in 1928) Indian physicists Raman and Krishnan carried similar experiments on the light scattering in liquids. In the first experiments, Indian scientists used sunbeam as a source of excitation radiation. By using certain combinations of absorptive filters, one came to the conclusion that light scattering followed by a frequency shift $\omega' = \omega_0 - \Omega_j$ (ω_0 - exciting radiation frequency, ω' - scattering light frequency) takes place in liquids. The results of their experiments were interpreted as a manifestation of the optical analogue of the Compton effect. This phenomenon was later called the Raman Effect. For the discovery of this phenomenon in 1930, Raman was awarded the Nobel Prize [1].

A study of a new type of light scattering from the early work immediately attracted the attention of wide circles of the scientific community. Undoubtedly, the discovery of this phenomenon is one of the most outstanding scientific achievements of the 20th century.

1.2 Elementary description

Raman scattering or combinational light scattering is an inelastic scattering of optical radiation on the molecules of matter (solid, liquid or gaseous), accompanied by a noticeable change in the frequency of the radiation. In contrast to the Rayleigh scattering in the case of Raman scattering in the spectrum of the scattered radiation extra lines appear apart from the main line of unbiased Fig.1. Number and arrangement of appeared lines are determined by the molecular structure of the substance.

Dipole moments associated with the distortion of the electron cloud of atoms are induced under the influence of an external electromagnetic field in a substance. It is possible to use a series expansion in the external electric field *E*:

$$p = \beta_1 \varepsilon_0 E + \beta_2 \varepsilon_0 E^2 + \beta_2 \varepsilon_0 E^3 + \cdots,$$

where $p -$ induced dipole moment of the atom; $\varepsilon_0 -$ absolute permittivity of the medium; $\beta_1, \beta_2, \beta_3 -$ appropriate linear and nonlinear susceptibilities.

Susceptibility $\beta_i = \beta_1, \beta_2, \beta_3, etc$ in turn depend on the location of the nuclei. Therefore, you can use their expansion in a series in the normal coordinate's η of nuclear vibrations:

$$\beta_i = \beta_i^{(0)} + \left(\frac{d\beta}{d\eta}\right)^{(0)}\eta + \left(\frac{d^2\beta_i}{d\eta^2}\right)^{(0)}\eta^2 + \cdots$$

The electric field can be represented in complex form

$$E = E_0 e^{-i\omega_0 t}$$

Where ω_0 – frequency electromagnetic radiation source. The vibrations of the nuclei must be harmonically. Accordingly, we can assume that $\eta = \eta_0 \cos \Omega_j t = \frac{1}{2}\eta_0\left(e^{-i\Omega_j t} + e^{i\Omega_j t}\right)$, where $\Omega_j -$ respective frequencies of the normal vibrations of the lattice. Accordingly, the induced dipole moment have

$$p = \beta_i^{(0)}\varepsilon_0 E_0 e^{-i\omega_0 t} + \frac{1}{2}\left(\frac{d\beta_1}{d\eta}\right)^{(0)}\varepsilon_0 E_0 \eta_0\left[e^{-i(\omega_0-\Omega_j)t} + e^{-i(\omega_0+\Omega_j)t}\right] + \beta_i^{(0)}\varepsilon_0 E_0^2 e^{-i\cdot 2\omega_0)t} + \frac{1}{2}\left(\frac{d\beta_2}{d\eta}\right)^{(0)}\varepsilon_0 E_0^2 \eta_0\left[e^{-i(2\omega_0-\Omega_j)t} + e^{-i(2\omega_0+\Omega_j)t}\right]$$

The expression takes into account only the lower coefficients of expansion in the external field E and the normal coordinate. The oscillating dipole moment in accordance with the general theory of radiation leads to radiation which frequency is equal to the frequency of the oscillations of the dipole moment. The first term corresponds to the scattering of light without changing the frequency (elastic or

Rayleigh scattering). The second term is due to Raman scattering occurring at the expense of the external field modulation optical vibrations with frequencies Ω_j. The third term is due to the scattering of light, accompanied by a doubling of the frequency $\omega' = 2\omega_0$ and called hyper-Rayleigh scattering of light. The fourth term is due to scattering at frequencies $\omega' = 2\omega_0 \pm \Omega_j$ (so-called hyper-Raman light scattering) [1].

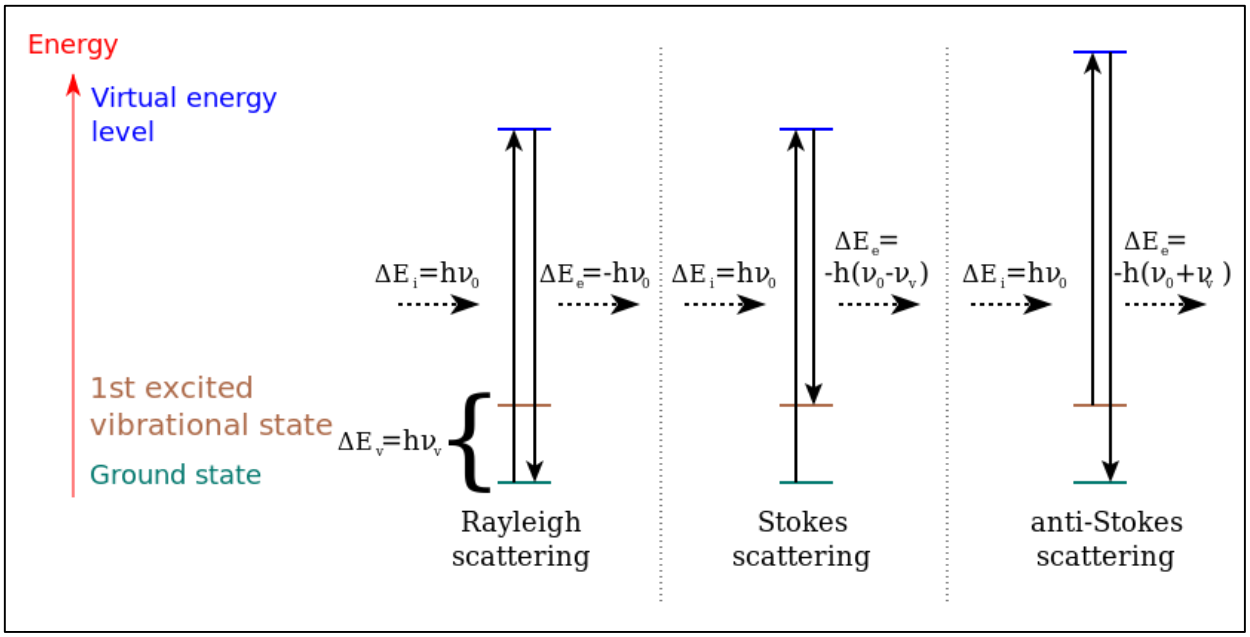

Figure 1 The different possibilities of light scattering: Rayleigh scattering (no exchange of energy: incident and scattered photons have the same energy), Stokes Raman scattering (atom or molecule absorbs energy: scattered photon has less energy than the incident photon) and anti-Stokes Raman scattering (atom or molecule loses energy: scattered photon has more energy than the incident photon)

2. Review of literature

The nanoparticles of iron oxide are a major focus of research in physics, chemistry, engineering and materials science, among others. Magnetite Fe_3O_4 has been subjected to a large number of studies employing different kinds of experimental techniques and theoretical approaches because its main magnetic properties such as superparamagnetism, high coercivity, low Curie temperature, high magnetic susceptibility, among others, which occur due to the nanometric size. The Fe_3O_4 nanoparticles can have various applications in nanotechnology, such as pigment, drug delivery, targeting, magnetic resonance imaging for clinical diagnosis, recording material, hyperthermia, catalyst, etc. [2,3]. Those nanoparticles have an ability to interact in different ways with different biological molecules due to their properties such as high specific area and wide variety of surface functionalization [4]. Yet, despite the intense effort and significant advances, understanding some of its fundamental properties still remains an elusive

goal. It is an internal interaction of structural, electronic, and magnetic properties that makes the studies on this compound so difficult. Effects of order–disorder of cations between octahedral and tetrahedral sites, nonstoichiometry, presence of impurities and defects, oxidation, sample history and origin (e.g., natural vs. synthetic crystals), have to be disentangled in order to reveal the genuine intrinsic properties. Vibrational spectroscopy, both infrared and Raman, proved to be a powerful tool for a direct probing of lattice dynamics of this compound, particularly in the temperature dependent studies of optical phonons across the Verwey transition [5].

Raman spectroscopy is a fast tool to distinguish iron oxides, hydroxides and oxyhdroxides. . In article [6] the main aim was to distinguish between the different iron oxides occurring in soils. Most of them can be identified by magnetic methods, but there are some minerals that are not easy to differentiate from each other. In these cases, the magnetic methods can be complemented by Raman spectroscopy. A severe problem is the fact that some iron minerals are transformed easily when applying laser powers of 1 mW or more. Most of the iron (oxy)hydroxides are converted to haematite and, consequently, it is impossible to identify the original material. Care has to be taken in these cases because Raman measurements are spot measurements that only analyse the surface at a specific location and not the bulk of the sample as most magnetic measurements do. However, Raman spectroscopy could be helpful in distinguishing magnetite and maghemite. Natural iron minerals are sometimes poorly crystallized and therefore transformrapidly during Raman measurements. Therefore, it is recommended that eachmeasurement startswith the lowest possible laser power. In most cases, the dominant minerals can be identified also at very low laser powers (0.01 mW)The spectra of magnetite and maghemite are sufficiently different. Magnetite shows bands at 310, 540 and 670 cm^{-1}, maghemite at 350, 500– 515, 665, 730 and 1330 cm^{-1}. Although small particles may not show the bands below 650 cm^{-1}, these can be distinguished by the double peak of maghemite around 700 cm^{-1} and by the 1330 cm^{-1} band, which does not appear in magnetite.

In article [4] nanoparticles of iron oxide (Fe_3O_4) were studied by Raman spectroscopy where spectrums were analyzed with different lasers: 514 nm (0.75 mW power used) and 785 nm (1.2 mW power used). The dominant structures of the spectra are in 215, 276, 398, 487, 654 and 1300 cm^{-1} when using the laser 514 nm. The spectrum produced with laser 514 nm is characteristic peak of magnetite in 654 cm^{-1}. The spectrum produced by laser 785 nm has a peak at 670 cm^{-1}, shifted relative to the laser 514 nm. The spectrum generated by laser 785 nm peaks characteristic of maghemite encountered due to possible oxidation of the sample caused by the high power laser.

Above the Verwey transition temperature ($T_v = 121$ K), the iron oxide magnetite $Fe^{3+}(Fe^{2+}Fe^{3+})O_4$ crystallizes in the cubic space group *Fd3m* (O_h^7), Z = 8: It represents the classical example of an inverse spinel ferrite AB_2O_4. Oxygen atoms, having general positions 32*e*; form approximately a close-packed face

centered cubic arrangement. The iron atoms occupy two crystallographically distinct sites being tetrahedrally A (8*a*) and octahedrally B (16*d*) coordinated by oxygen anions. The inverse nature of this spinel implies that the *A*-sites are occupied by Fe^{3+} ions, while an equal number of Fe^{2+} and Fe^{3+} cations share the *B*-site.

Polarized Raman study on oriented single crystals represents a powerful tool for deducing the symmetry of vibrational modes. The primitive unit cell of magnetite contains one $Fe_4^{2.5+}$unit where iron atoms are coordinated octahedrally (D_{3d}), and two $Fe^{3+}O_4^{2-}$units with the tetrahedral coordination (T_d). Group-theoretical and lattice-vibration analyses based on the quasimolecular description of the spinel structure have led to the following description of normal mode motions of the FeO_4 tetrahedron [7]: A_{1g}—symmetric stretch of oxygen atoms along Fe–O bonds, E_g and $T_{2g}(3)$—symmetric and asymmetric bends of oxygen with respect to Fe, respectively, $T_{2g}(2)$—asymmetric stretch of Fe and O, $T_{2g}(1)$—translatory movement of the whole FeO_4. There are zero, or close-to-zero displacements of Fe atoms in modes A_{1g}; E_g; and $T_{2g}(3)$. Polarized experiments on the oriented single crystal provide a new interpretation of the Raman spectrum with the following assignment for symmetries of the observed modes: A_{1g} for 668 rcm^{-1}, E_g for 306 rcm^{-1}, and T_{2g} for 538 rcm^{-1}, 193 rcm^{-1}, and 450–490 rcm^{-1}.

Moreover it was revealed that for a powdered magnetite laser power well below 25mW caused a rapid oxidation. The first recognizable features of hematite appeared at about 300 and 410 rcm^{-1}. Upon further increase of laser power their intensity grew dramatically and dominated the spectra. We also found that the Raman scattering power of hematite is much larger that the scattering power of magnetite. As a result, even a very small amount of hematite causes the presence of spurious peaks in the Raman spectrum of magnetite [5].

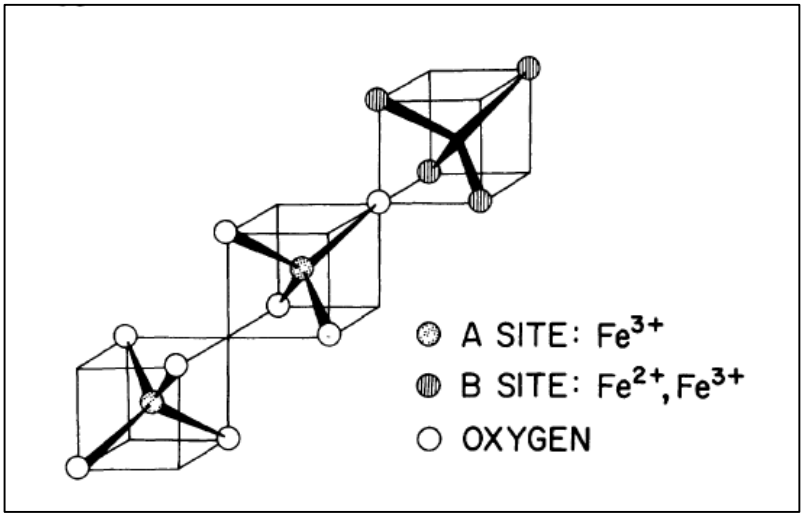

Figure 2 Illustration of fourteen atoms in the primitive unit cell for the cubic phase of magnetite. The bonds drawn between atoms are intended to indicate the tetrahedral symmetry of molecular units.

Verble [7] has obtained and identified the normal modes of vibrations using a molecular model, which takes into account the tetrahedral symmetry of molecular units in the crystal of magnetite. The molecular model of Waldron who was the first to propose that the vibrational modes of ferrites of the type B_2AX_4 could be treated in terms of three individual units of tetrahedral symmetry. His approach was to group the 14 atoms per unit cell into one B_4 tetrahedron and two AX_4 tetrahedra. In Fe_3O_4 this grouping leads to one Fe_4 and two FeO_4 units Fig.2.

The normal modes of the isolated molecular unites can be specified as follows. For each of the AX_4 tetrahedra, there are 1 A_1, 1 E, 1 T_1, and 3 T_2 modes. These classified translational, rotational, or internal as indicated in Table I. The single B_4 unit is equivalent to a tetrahedral molecule without its central atom. The normal modes in this case are therefore 1 A_1, 1E , 1T_1 and 2T_2 the frequencies of the A_1, E, T_2^2, and T_2^3 modes are represented respectivele by ν_1, ν_2, ν_3, and $\nu 4$.

Table I Classification of molecular modes for the spinel lattice.

	Translational	Rotational	Internal
$2AX_4$	$2T_2$ (6)	$2T_1$ (6)	$2A_1 + 2E + 4T_2$ (18)
B_4	$1T_2$ (3)	$1T_1$ (3)	$1A_1 + 1E + 1T_2$ (6)

For the purpose of illustration Fig. 2, 3 show the normal vibrations for five Raman-active modes, namely the A_{1g}, E, and $3T_{2g}$ modes. On the basis of the symmetry coordinates shown in Fig. 3, 4 together with a knowledge of the frequencies of several of the infrared-active modes, it is possible to identify the symmetry coordinates associated with the five experimentally observed Raman-active modes.

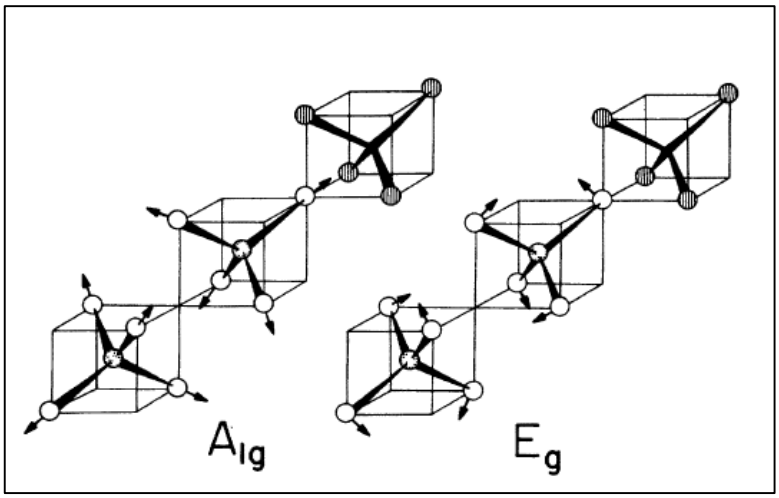

Figure 3 Normal vibrations of the A_{1g} and Eg modes in the cubic phase of magnetite.

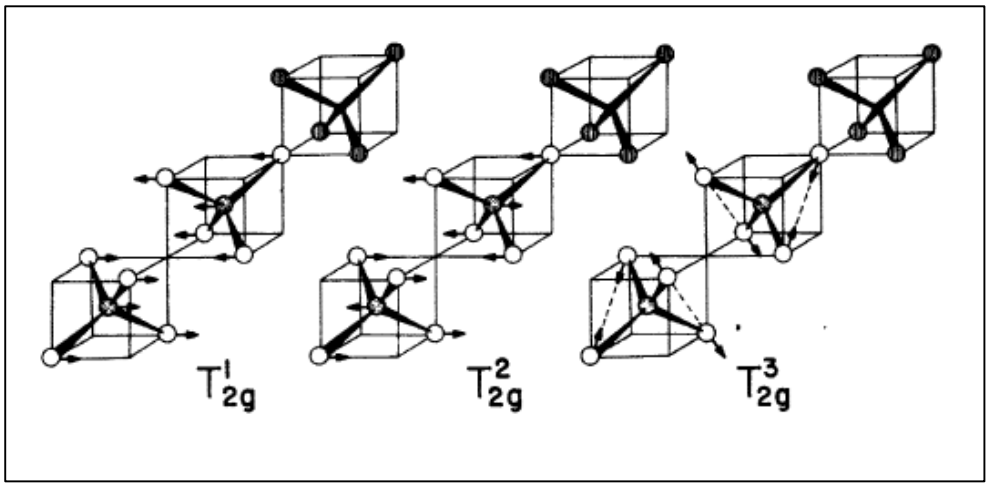

Figure 4 Normal vibrations of the 3 T_{2g} modes in the cubic phase of magnetite.

In magnetite, exist a close correspondence between the frequencies of the associated infrared and Raman modes. In the article the 565 cm^{-1} ir mode with the 560 cm^{-1} Raman mode and the 360 cm^{-1} ir with the 320 cm^{-1} Raman mode was paired. This pairing implies that both of these Raman-active phonons have T_{2g} symmetry. Furthermore, since in the molecular case it was expected the A_1 mode to have one of the two highest frequencies, so A_{1g} symmetry was assigned to the 680 cm^{-1} vibration. The remaining T_{2g} mode is an external-type vibration which pairs with the external translational (acoustical) mode; therefore, it was assigned this symmetry to the lowest frequency (300cm^{-1}) phonon. Only the E_g phonon remains out of the original five and was assigned to the 420 cm^{-1} mode. The activity and frequencies of the optical active modes in magnetite are listed in columns 3 and 4 of Table II.

In order to explain the broadening of Raman line of magnetite a model has been proposed in which static and dynamic electronic disorder are the two most important concepts.

The case of static disorder can be treated according to the theory of Kawamura, Tsu, and Esaki [8]. In discussing the Raman-scattering process from an electronically disordered alloy system, these authers point out that momentum is no longer conserved in the electronic intermediate states. The electron wave function, which are perturbed by the disorder, take the form

$$\psi_k(\vec{x}) = \sum_G A_G\, e^{i(\vec{k}+\vec{G})\cdot\vec{x}} + \int g(\vec{k}-\vec{k}')\, e^{i\vec{k}'\cdot\vec{x}} d^3k' =$$

$$= \Phi_k(\vec{x}) + R_k(\vec{x})$$

where the first term represents a Bloch contribution and the second term is a random function arising from the disorder. As a consequence of this latter contribution, the matrix elements contained in the expression for the Raman cross section are found to involve terms resulting from momentum nonconserving processes. The Raman cross section itself is found to be propotional to the phonon density of states and to depend on the square of the spatial charge-density fluctuations arising from the random part of the electronic functions.

Table II Classification of the normal modes of magnetite (cubic phase).

Molecule	Crystal	Activity	Freq. (cm^{-1})	Classification	Ions involved	Molecular freq.
A_1	A_{2u}^1			Int.	$B+O$	ν_1, ν_1, ν_1
	A_{2u}^2			Int.	$B+O$	ν_1, ν_1, ν_1
A_1	A_{1g}	Raman	680	Int.	O only	$\nu_1, \nu_1, 0$
E	E_u^1			Int.	$B+O$	ν_2, ν_2, ν_2
	E_u^2			Int.	$B+O$	ν_2, ν_2, ν_2
E	E_g	Raman	420	Int.	O only	$\nu_2, \nu_2, 0$
T_1	T_{2u}^1			Rot., Ext.	$B+O$	$\nu_{Rot}, \nu_{Rot}, \nu_{Rot}$
	T_{2u}^2			Rot., Ext.	$B+O$	$\nu_{Rot}, \nu_{Rot}, \nu_{Rot}$
T_1	T_{1g}			Rot., Ext.	O only	$\nu_{Rot}, \nu_{Rot}, 0$
	T_{1u}^1	Acoust.		Trans., Ext.	$A+B+O$	ν_0, ν_0, ν_0
T_2	T_{2g}^1	Raman	300	Ext.	$A+O$	$\nu_0, \nu_0, 0$
T_2	T_{1u}^2	ir	178	Ext.	$A+B+O$	ν_0, ν_0, ν_0
	T_{1u}^3	ir	565	Int.	$A+B+O$	$\nu_3, \nu_3, 0$
T_2	T_{2g}^2	Raman	560	Int.	$A+O$	$\nu_3, \nu_3, 0$
T_2	T_{1u}^4	ir	268	Int.	$A+B+O$	ν_4, ν_4, ν_4
	T_{1u}^5	ir	360	Int.	$A+B+O$	ν_4, ν_4, ν_4
T_2	T_{2g}^3	Raman	320	Int.	$A+O$ (O only)	$\nu_4, \nu_4, 0$

It should take into account the difference between alloy substitutions and Fe_3O_4. In magnetite it is the random arrangement of multivalent iron atoms (Fe^{2+} and Fe^{3+}) on the octahedral *B* sites which gives rise to the electronic disorder. Fe^{2+} and Fe^{3+} ions in magnetite are differ significantly in their ionic and chemical properties. In contrast to the compositional disorder of the alloy systems, chemical disorder involves a change in the outermost shells of electrons but no change in the ions cores. A possible consequence of this might be an enhanced effect of disorder on light scattering. This type of disorder should give rise to on intermediate electronic states for which momentum is a poorly defined quantity. Electronic disorder for Fe_3O_4 is not complete but is only partial. This is due to the fact that only the B-site ions are involved in the disorder and rest of the lattice is assumed to be perfect. As a result, only a 'partial' breakdown in the momentum selection rules. That lead to an energy-broadened phonon density of states, which is reflected in the Raman spectrum as broadened Raman lines. Thus, the phonon

linewidth in Fe_3O_4 provide a measure of the degree of electronic disorder in the system.

Dynamic disorder in magnetite at temperatures between T_v and 400K is interpreted in terms of the small-polaron model of Camphausen and Chakraverty [9]. The transport properties are assumed to be dominated by near-neighbor small polaron hopping due to phonon-assisted processes.

The small-polaron-hopping process can be characterized by hopping time t_h. it has been estimated this hopping time to be 3.5×10^{-15} sec at 300K. phonon lifetime influence only if the polaron-hopping time is shorter than (or the order of) the period associated with the phonon involved, i.e., $\omega_0\ t_h \lesssim 1$, where ω_0 is the angular frequency of the phonon. Otherwise, the polaron do not have time to redistribute themselves between oscillations and no effect can be observed. Using the room temperature value for t_h and ν_0=680 cm^{-1} for A_{g1} phonon $\omega_0\ t_h$=0.45. The value of t_h is sufficiently short to meet the criterion and this suggests that polaron hopping is the dominate temperature dependent broadening mechanism.

Camphausen and Chakraverty found experimentally that as the carrier density of their p-type samples was raised, the Raman lines broadened considerably and shifted to lower phonon frequencies. Both effects were attributed to splitting of the valance band by an electron-phonon interaction involving q-0 optical phonons. Of special importance to these results is the fact that, in the presence of a lattice vibration, a finite time is required for the carriers to come into thermal equilibrium. The maximum effect on the phonons occurs when $\omega_0\ \tau \cong 1$, where τ is the free-carrier redistribution time. For this case, one can find that there is a dynamic-frequency shift in the Raman line given by

$$\delta\omega_r = \delta\omega_s/[1 + (2\omega_0\tau)^2]$$

Where $\delta\ \omega_s$ is the frequency shift defined for the case of a static strain, i.e., where $\omega_0\ \tau \ll 1$. There also occurs a contribution to the linewidth which is due to the dynamics strain associated with an optical phonon and which is given by

$$\Gamma = \delta\omega_s(2\omega_0\tau)/[1 + (2\omega_0\tau)^2]$$

These formulas imply that the maximum broadening should occur for $2\omega_0\ \tau=1$ and that the frequency shift is substantially reduced over a broad range $2\omega_0\ \tau=1$. In the assumption that one can apply these formulas to the present situation and replace τ by t_h then one finds that the condition $2\omega_0\ \tau=1$ (actually $2\omega_0\ t_h$=0.9) is almost exactly satisfied at room temperature.

3. Facility description

A scanning confocal laser Raman microspectrometer “Confotec CARS” coupled with a NIKON TE2000-E inverted microscope and employing two microobjectives 40x-0.6NA and 60x-1.2NA are used to acquire all of the Raman spectra Fig.5. The 520 cm^{-1} band of a silicon wafer was used for frequency

calibration. Three color lasers are installed at the optical platform for Raman scattering studies. The excitations at 633 and 532 nm were provided by a He-Ne laser (Melles Griot 05-LHP-991) and a diode laser with an adjustable output power (model SLM-417-20) respectively. The excitation at 785nm was provided by 85 MHz passively mode-locked picosecond laser (model EKSPLA, PT257-SOPO) tunable in the range of 690-990nm. A selection of dichroic mirrors, clean-up, and edge filters from Semrock were used in association with 532nm, 633nm and 785nm excitation wavelengths.

Figure 5 General view of the "Confotec CARS" microscope

The average laser power on the sample is controlled by a variable neutral filter with the 0–3 optical density which allows to range the power from few μW to tens of mW. The excitation light was focused on the sample in ~ 1 μm laser spot (40x) or ~ 650 nm laser spot in the case of water emersion objective with high NA.

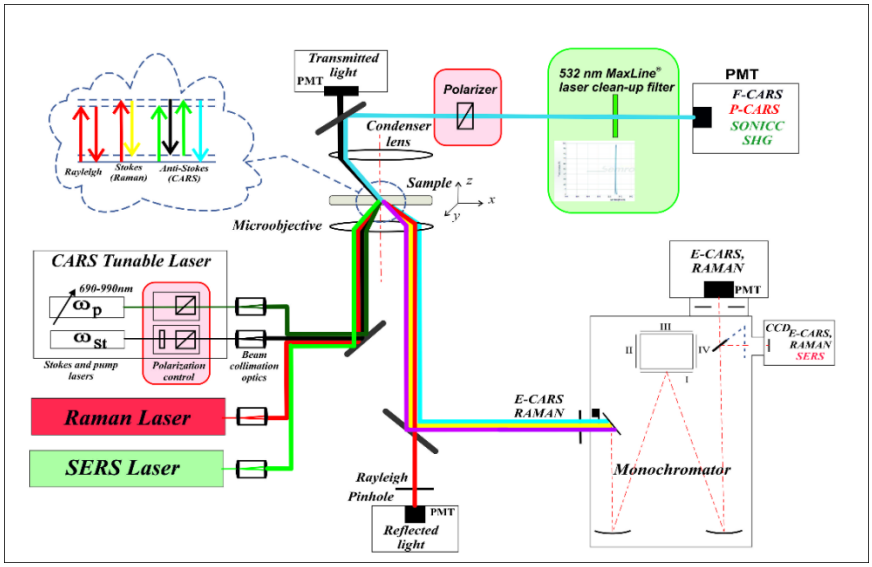

Figure 6 Layout of the "Confotec CARS" microscope

The Raman signals from the analytes, located at the motorized sample position adjustment stage (Prior Scientific, H117TE), are collected in epi-direction, dispersed by monochromator-spectrograph MS520 with a 600 grooves/mm grating and detected with a Peltier-cooled CCD camera (ProScan HS−101 H) cooled to −20 °C. Usually spectra are collected at different localizations of the samples with an integration time of (1-30)s with a spectral resolution of 2.0cm-1. A screen image recorder camera attached to the microscope enabled the acquisition of the white-light micrographs of the area under investigation.

4. Results and discussions

4.1 Experimental Raman spectra of magnetite

All Raman spectra of synthesized magnetite were recorded at room temperature upon laser excitations operating at 633 and 785 nm. Samples were illuminated through objectives 40x or 60x with high numerical aperture. The acquisition time varied from 10 to 30s.

The obtained spectra are typical for small particles of magnetite: they consists of four Raman – active phonon modes. Oxygen phonon modes usually have their frequency above 200 cm^{-1}, whereas vibrations of the heavier iron atoms should be at much smaller frequencies. Two T_{1u} oxygen modes were recorded near 350 cm^{-1} and 560 cm^{-1}. The strongest peak at ≈670 cm^{-1} is assigned as A_{1g} mode which has the highest Raman shift as it involves the stretching vibrations of the oxygen atoms along the Fe(A)-O bonds. Peaks at 193 cm^{-1}, 308 cm^{-1}, and 540 cm^{-1} correspond to three T_{2g} modes. The large linewidth of magnetite Raman bands are due to the electronic disorder. In magnetite the random arrangement of multivalent iron atoms on the octahedral B – site increases the electronic disorder. Broadening mechanism is explained in details in the article by Verble [7].

The fingerprint peak of magnetite at 682 cm^{-1} in the spectrum recorded upon laser excitation at 633nm is presented in Fig 7 (a,b). While in the case of 785nm excitation this peak is shifted to 640 cm^{-1} Fig 8 (a,b). This can be interpreted by possible oxidation of the sample caused by the high laser power. Moreover, the intensity of this peak decreases for 3-4 orders of magnitude for spectrum generated at 785nm laser with respect to the one at 633nm laser. The received results are in good agreement with the literature data [4,10]

To increase the spectral resolution of our experiments we also performed our measurements employing 60x objective with NA=1.2. This allows distinguishing peaks at 190 cm^{-1} and shoulder centered around 537 cm^{-1}. Furthermore, one can observe increase of the intensity in the spectrum recorded upon 785 nm laser excitation with this objective.

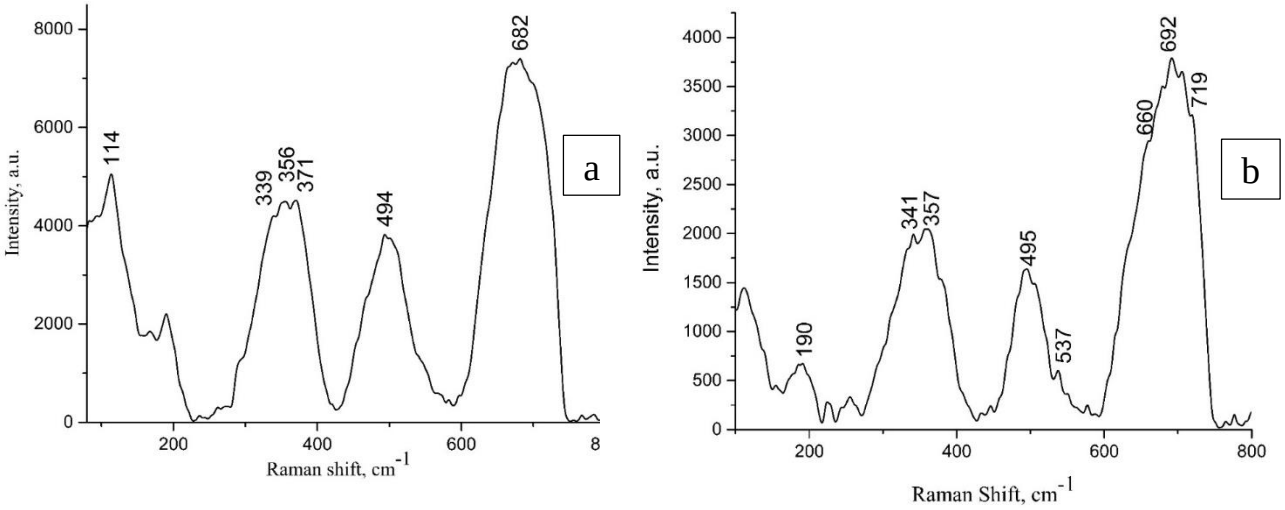

Figure 7 Raman spectrum of synthesized magnetite powder recorded upon 633 laser excitation employing a) 40x b) 60x objectives

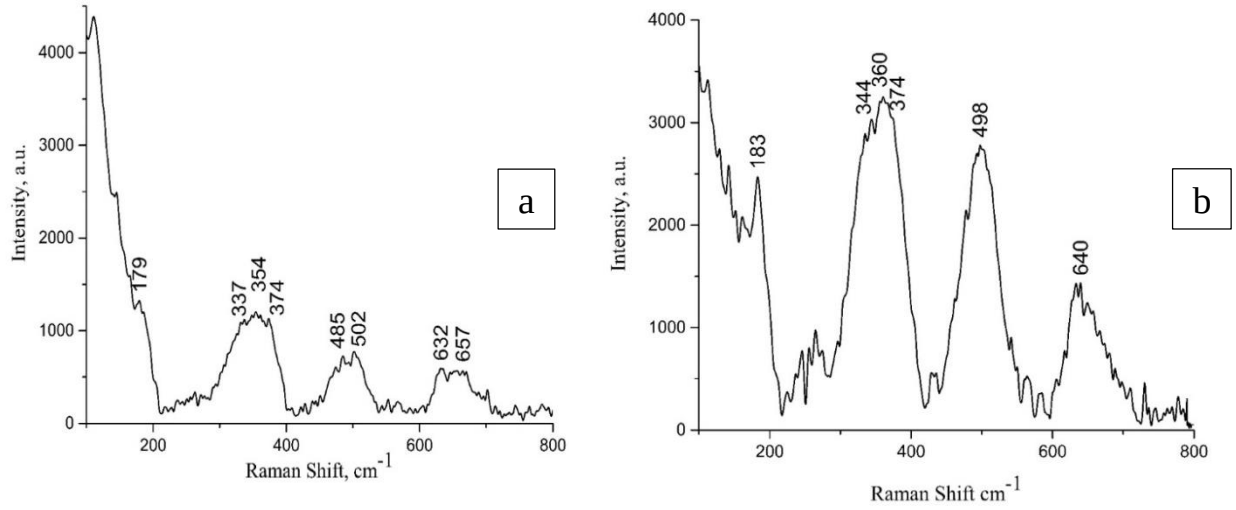

Figure 8 Raman spectrum of synthesized magnetite powder recorded upon 785nm laser excitation employing a) 40x b) 60x objectives

4.2 Phase transitions

It is known that bivalent iron makes magnetite easily prone to oxidation [11]. A thorough study was made on the effect of laser power influence on Raman spectrum of powdered synthetic magnetite.

In this study, the laser power was smoothly varied with the use of neutral filters in order to detect the threshold of the oxidation which results in the phase transition. We didn't observe any changes in Raman spectra at the level of laser power up to 1.06 mW. Further stepwise increase in power alerts the Raman spectra, which was attributed to oxidation of the sample Fig.9.

Some important phase transition details are presented in the Fig.10. For instance, it is clearly seen that the threshold power is close to be at the level of

1.3mW as some changes in the small wavenumber part of the Raman spectrum are recorded: the ratio of 355 cm^{-1} and 490 cm^{-1} peaks intensities changes and the intensity of the peak at 246 cm^{-1} starts to increase. At the power of 1.6mW the phase transition is obvious and the maghemite spectrum is obtained. Subsequent exposure of the sample during 30s or more at the same power of 1.6mW leads to the one more phase transition process: characteristic hematite spectrum with Raman peaks located at 225, 288, 406, 490, 609, 1300 cm^{-1} is recorded, being in a good agreement with literature [6,10].

Gallagher has proposed the model that describes the oxidation mechanism for small particles of magnetite [11]. It was predicted that during oxidation a high concentration gradient of cation holes would develop in the monocrystalline particles, leading to a gradient in the lattice constant; thus lattice strain would develop. Hence the lattice strain was assumed to be the driving force for the nucleation of α-Fe_2O_3. For small particles the difference in the concentration gradient on the surface and in the core of a particle is responsible for the change in the lattice parameters promoting the strain development.

To summarize the above, it should be noted that the first step of the oxidation of the powdered magnetite involves the formation of the metastable iron oxide maghemite, which transforms to the final product hamatite under the continuing exposure of the laser excitation. These transformations are irreversible.

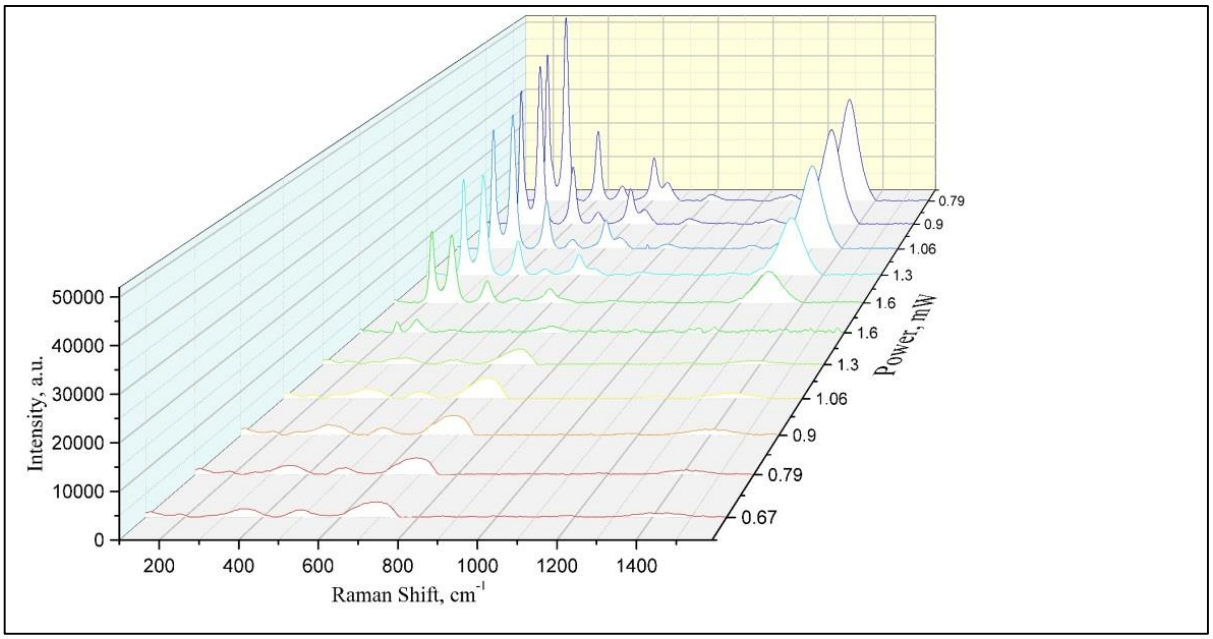

Figure 9 Raman spectra of the sample at different laser powers. Excitation – 633nm

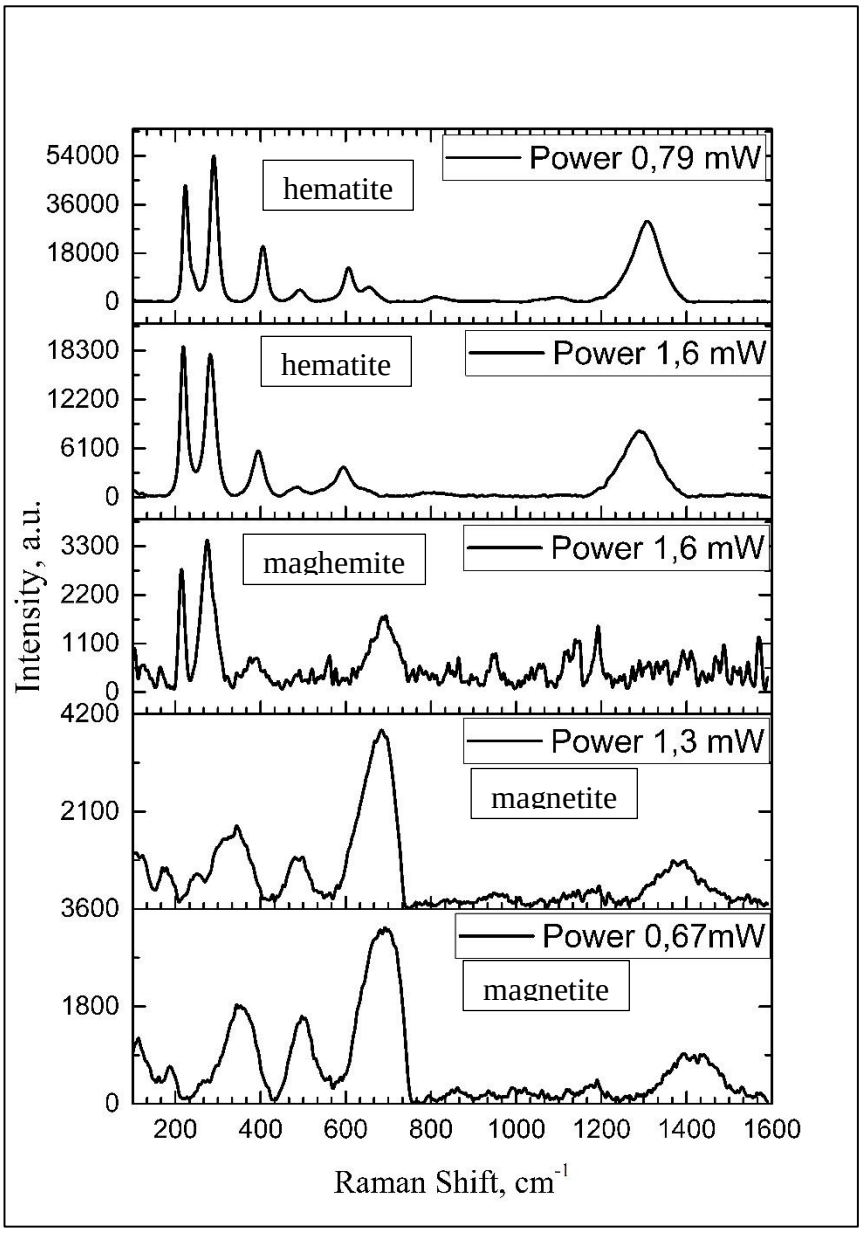

Рисунок 10 Raman spectra demonstrating phase transition processes vs laser power

4.3 Bacterial reduction study

Two samples were prepared: control sample of synthesized magnetite that was kept in the bacterial medium and experimental sample that was obtained during the growth of dissimilatory iron-reducing bacteria [12]. We performed studies of these samoles by Raman spectroscopy.

Raman spectra were measured at 5 randomly distributed locations on the sample to avoid the results to be influenced by the operator (for instance, by choosing only similar looking locations). The obtained spectra were the same at all of these locations.

Raman spectra of these samples were recorded upon laser excitations at 633nm and 785nm by employing 60x objective Fig 11. The spectra consist of 4 intrinsic for magnetite peaks with the similarity between the control sample and the experimental one, except the intensity of the peaks which are stronger for the last

one. The intensity increase might be due to the crystallinity improve which could be caused by bacterial growth resulting in the decrease of vacancies.

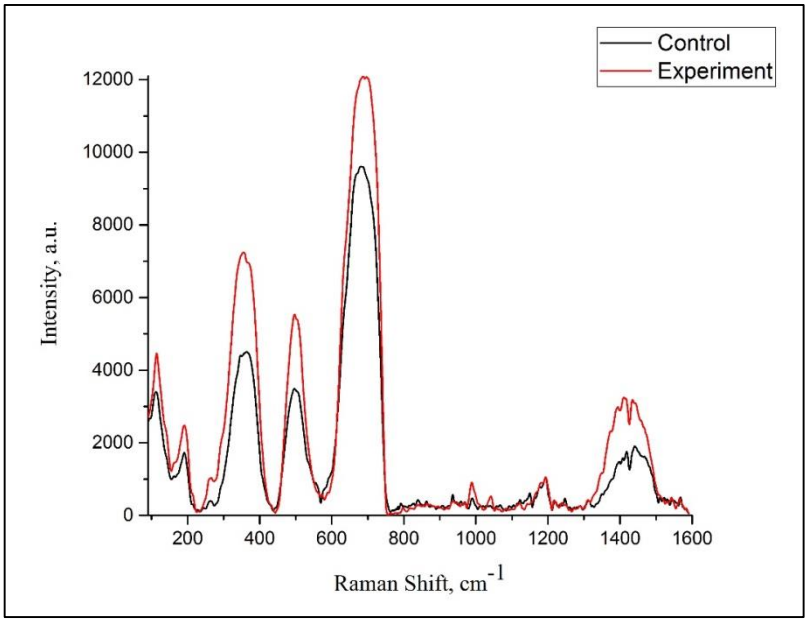

Figure 11. Comparison Raman spectra of control and experimental samples, excitation 633nm

We consider that the further studies on this matter could be of big scientific interest.

Conclusion

During the summer student program at JINR I have been acquainted with a unique facility – laser confocal scanning "CARS" microscope located at the Sector of Raman Spectroscopy, Laboratory of Neutron Physics. The activities were focused on the Raman spectroscopy studies of powdered magnetite using two-color laser excitations at 633nm and 785nm. Along with the measurements of standard magnetite Raman spectra, we performed a set of experiments to found out some specific peculiarities of magnetite behavior upon the laser excitation with varied power. In particular, we observed and recorded phase transition processes like magnetite-meghemite-hematite under the 633nm laser excitation with different power and exposure time. Also, we started experiments to study bacterial reduction phenomena and got the very first preliminary results which needs their further investigation.

Concluding my report I'd like to express my gratitude to the whole staff members of the Raman spectroscopy sector and special thanks to my supervisor Dr Grigory Arzumanyan for his great attention and care of my practice work. I'm also grateful to JINR University Centre for providing me such a nice opportunity to work in one of the JINR's laboratories.

Literature

1 Gorelik V.S., Combinational light scattering // ISSEP, 1997, 6.

2 Sun, J., *et al*., Synthesis and characterization of biocompatible Fe_3O_4 nanoparticles // Journal of Biomedical Materials Research Part A, 2007, **80A**, 2.

3 Wu, W., *et al*., Magnetic Iron Oxide Nanoparticles: Synthesis and Surface Functionalization Strategies // Nanoscale Research Letters, 2008, **3**, 11.

4 Panta PC and Bergmann CP, Raman Spectroscopy of iron oxide of nanoparticles (Fe_3O_4) // Material Science & Engineering, 2015, **5,** 1.

5 Shebenova O.N. and Lasor P, Raman spectroscopic study of magnetite ($FeFe_2O_4$): a new assignment for vibrational spectrum // Solid State Chemistry, 2003, 174

6 Hanesh M., Raman spectroscopy of iron oxides and (oxy)hydroxides at low laser power and possible applications in environmental magnetic studies // GJI, 2009, 177.

7 Verble J.L., Temperature-dependant light-scattering studies of the Verwey transition and electronic disorder in magnetite // Physical Review, 1973, **9**, 12.

8 Kawamure H., et al., // Physical review letters, 1972, **29**, 1397

9 Campausen D.L. and Chakraverty B.K., // Proceedings of the eleventh International conference on the physics of semiconductors,Warsaw,1972

10 Shebanova O.N. and Lazor P., Raman study of magnetite (Fe_3O): laser-indeced thermal effects and oxidation // Journal of Raman Spectroscopy, 2003, 34

11 Gallagher J, et al., Mechanism of oxidation of magnetite to γ-Fe_2O_3 // Nature (London), 1968, 217

12 Zavarzina D.G.et al., *Geolkalibacter ferrihydriticus* gen. nov. sp. nov. the first alkakaphilic representive of the family *Geobacteracea*, isolated from a soda lake // Microbiology, 2006, **75**, 6